Vehement Competition of Multiple Superexchange Interactions in Cu(OH)F

Igor Danilovich,[1] Anna Merkulova,[1] Anastasia Polovkova,[1] Elena Zvereva,[1] Yevgeniy Ovchenkov,[1] Igor Morozov,[1] Badiur Rahaman,[2] Tanusri Saha-Dasgupta,[3,*] Christian Balz,[4] Hubertus Luetkens,[5] and Alexander Vasiliev[1,6,7,#]

[1]Moscow State University, Moscow 119991, Russia
[2]Aliah University, Kolkata 700156, India
[3]S.N. Bose National Centre for Basic Sciences, Kolkata 700098, India
[4]Helmholtz-Zentrum Berlin for Materials and Energy, 14109 Berlin, Germany
[5]Laboratory for Muon-Spin Spectroscopy, Paul Scherrer Institute, 5232 Villigen, Switzerland
[6]Ural Federal University, Ekaterinburg 620002, Russia
[7]National University of Science and Technology "MISiS", Moscow 119049, Russia

The mixed anion copper compound Cu(OH)F was studied in measurements of magnetic susceptibility, static and pulsed field magnetization, specific heat, X-band electron magnetic resonance and muon-spin spectroscopy. In variance with its layered structure, the magnetic behavior shows no evidence of low-dimensionality. Cu(OH)F reaches short range static antiferromagnetic order at T_N = 9.5 ÷ 11.5 K and experiences the spin-flop transition at B ~ 3.5 T. This behavior is in a sharp contrast with physical properties of earlier reported isostructural compound Cu(OH)Cl. The first principle calculations reveal highly competitive nature of ferromagnetic and antiferromagnetic superexchange interactions, the details being rather sensitive to choice of magnetic structure employed in the extraction of magnetic interaction. Rather broad anomaly in $C_p(T)$ dependence at phase transition and smeared magnetization curve M(B) at low temperatures suggest static disorder in the ground state. Zero-field μSR data are consistent with Cu(OH)F experiencing a transition into a static magnetically disordered state.

1. Introduction

Among numerous building blocks of inorganic chemistry the polyhedral units of divalent copper in oxygen coordination attract most attention in a quest for low dimensional magnetism and superconductivity.[1)] The copper polyhedra appear to be heavily distorted due to Jahn – Teller effect inherent for electronic $3d^9$ shell of Cu^{2+} ions. The pseudo-octahedral coordination units CuO_6 may differ in their distortion. It could show symmetric or asymmetric shortening and elongation of basal and apical bonds. The positions of the apical ligands may heavily deviate from the normal to the basal plane and the basal plane itself may be bent. In this sense, better description for these units could be given in terms of pyramids CuO_5, pseudo-tetrahedral CuO_4 units or planar squares CuO_4.[2)] The lower coordination of copper facilitates the reduced dimensionality of magnetic subsystem in the crystal structure. In complex oxides, the copper polyhedra linked through corners, edges or faces frequently form isolated chains or layers separated by nominally non-magnetic structural units. These quasi-one-dimensional and quasi-two-dimensional structures develop short-range correlations but may be prevented from reaching a long-range magnetic ordered state. The non-magnetic units providing rather efficient pathways for the exchange interactions help to overcome this difficulty which may result in formation of three-dimensional magnetic order at lowering temperature.[3)] Similarly the tendency to form low-dimensional magnetic structures is rather pronounced in complex cupric halides and the role of side groups is also important in these compounds.

Despite the fact, that both cupric oxide CuO and cupric halides CuX_2 (X = F, Cl, Br) have been the topic of research due to their low dimensional magnetic structures, there is renewed interest in these compounds. To some extent, this is due to observation of multiferroicity in these compounds.[4-6)] In spite of their chemical simplicity, the magnetism in cupric oxide and cupric halides is rather tricky. The structure of copper monoxide, CuO, is monoclinic of space group *C2/c*. Each copper is coordinated to four coplanar oxygens at the corners of a square. The CuO_4 squares form infinite ribbons which are linked to adjacent chains by sharing corners.[7)] CuO reaches the magnetically ordered state through succession of three distinct antiferromagnetic phase transitions into

incommensurate collinear structure at T_{N3} = 229.8 K, incommensurate spiral structure at T_{N2} = 229.2 K and commensurate collinear structure at T_{N1} = 213 K.[8,9] The broad maximum in magnetic susceptibility found near 550 K has been treated as manifestation of linear chain antiferromagnetism.

Both $CuCl_2$ and $CuBr_2$ crystallize in a CdI_2-type structure with a monoclinic lattice of space group *C2/m***.** This crystal structure consists of $CuCl_2$ ($CuBr_2$) slabs made up of $CuCl_2$ ($CuBr_2$) chains. The slabs are interconnected via van der Waals interactions. The copper chloride (bromide) shows one-dimensional antiferromagnetic behavior and reaches magnetically ordered state at T_N = 23.9 K (73.5 K).[10,11] The incommensurate spiral antiferromagnetic structure in these halides results from competing ferromagnetic nearest-neighbor and antiferromagnetic next-nearest-neighbor exchange interactions along the spin chains. The copper fluoride CuF_2 crystallizes in a monoclinically distorted rutile structure of $P2_1/c$ space group with square planar coordination of copper by fluorine. It is canted antiferromagnet with Neel temperature T_N = 69 K.[12] It was established that the antiferromagnetic order arises from the coupling of one-dimensional subunits which themselves exhibit a very small ferromagnetic coupling between Cu neighbor cations.[13]

In the list of "simplest" cupric compounds are less investigated cupric hydroxide $Cu(OH)_2$ and mixed hydroxide halides Cu(OH)X, which needs attention. The crystal structure of non-centrosymmetric $Cu(OH)_2$ is orthorhombic of $Cmc2_1$ space group. The copper ions in this compound are in a strongly distorted octahedral environment. The chains of octahedra build up the corrugated layers by sharing edges of apical and equatorial hydroxide ions.[14] Concerning magnetism in $Cu(OH)_2$ it is established only that it shows typical low-dimensional antiferromagnetic behavior,[15] and orders at T_N = 21 K.[16]

The mixed anion copper based compounds are cupric hydroxide halides Cu(OH)Cl and Cu(OH)F. The copper hydroxide chloride crystallizes in monoclinic space group $P2_1/c$.[17] It was found that the magnetic properties of Cu(OH)Cl can be described by a quasi-two-dimensional spin model. Layers of divalent copper ions are arranged in a distorted Shastry-Sutherland lattice, i.e. square lattice with extra diagonal bonds that introduce frustration. The cupric hydroxide chloride orders antiferromagnetically at T_N = 11 K.[18] In this stidy, we present the first experimental and theoretical study of magnetism in Cu(OH)F.

2. Experimental

The structure of Cu(OH)F is shown in Fig. 1. It is formed by corrugated layers of edge-sharing $Cu(OH)_3F_3$ polyhedra in the *ab* plane which are interconnected by hydrogen bonds along the *c* axis. The ions of divalent copper Cu^{2+} are octahedrally coordinated, these units are heavily distorted due to the Jahn-Teller effect. The vertexes of octahedra are occupied by three fluorine ions F^{1-} and three oxygen ions O^{2-} belonging to hydroxyl groups OH^-.[19]

The synthesis of copper (II) fluoride hydroxide, Cu(OH)F, was carried out in accordance with the reaction $CuF_2 + H_2O = Cu(OH)F + HF$. All treatments with solutions containing fluorine ions were performed in a Teflon ware. To prepare the precursor CuF_2 $2H_2O$ the copper carbonate hydroxide, $Cu_2(OH)_2CO_3$, was dissolved in the excess of hydrofluoric acid water solution under heating and stirring with subsequent filtration and evaporation upon cooling. Then, the hydrolysis of CuF_2 $2H_2O$ was undertaken by the boiling and stirring of saturated water solution. It is important to note that throughout the process in the system remained an excess of solid CuF_2 $2H_2O$. The final product as the precipitate of the light olive color was separated from the solution and washed repeatedly with water to remove residual CuF_2. Separation of the precipitate from the solution was carried out by centrifugation. In the final stage the precipitate was washed twice with acetone and dried in air. By powder X-ray diffraction (XRD), it was found that the resulting sample is a single phase. The XRD pattern did not contain impurity lines, the monoclinic unit cell parameters found as a result of indexing were in agreement with published data.[19]

Electron spin resonance (ESR) studies were carried out using an X-band ESR spectrometer CMS 8400 (ADANI) (f~9.4 GHz, B~0.7 T) equipped with a low temperature mount, operating in the range T=5-300 K. The effective g-factor has been calculated with respect to a BDPA (*a,g* -bisdiphenyline-*b*-phenylallyl) reference sample with g_{et}=2.00359. The measurements of

thermodynamic properties, i.e. magnetic susceptibility χ, magnetization M and specific heat C_p were done on pressed (not sintered) pellets using "Quantum Design" Physical Properties Measurements System PPMS-9T. The pulsed magnetic field measurements were done on home-made magnetometer and calibrated using the PPMS data. Zero-field μSR measurements were performed on a pressed pellet of Cu(OH)F at the GPS spectrometer at the Laboratory for Muon Spin Spectroscopy, Paul Scherrer Institute, Switzerland.

3. Electron spin resonance

The temperature evolution of the powder ESR spectra of CuOHF is shown in Fig. 2. Over the whole temperature range studied the ESR powder pattern is characteristic of Cu^{2+} ions with an anisotropic *g*-tensor, while the hyperfine structure expected from natural ^{63}Cu and ^{65}Cu isotopes (I=3/2) is suppressed, presumably due to the presence of weak exchange interactions. The amplitude of signal increases monotonously upon cooling the sample down to ~ 15 K, then the signal weakens in amplitude and eventually its degradation occurs, which is indicative of the onset of static magnetic order at low temperatures.

In order to evaluate the main ESR parameters of the line we have fitted the experimental spectra by sum of two components corresponding to the principal values of the *g*-tensor in accordance with Lorentzian function of the type

$$\frac{dP}{dB} \propto \frac{d}{dB}\left[\frac{\Delta B}{\Delta B^2 + \left(B - B_r\right)^2}\right] \qquad (1)$$

where P is the power absorbed in the ESR experiment, B is the applied magnetic field, B_r is the resonance field and ΔB is the linewidth. The results of fitting are shown by red solid lines in Fig. 2. A representative fit of the ESR data is given in Fig. 3(a) with the resolved resonance modes denoted by dashed lines and their sum is shown by the solid line. The temperature dependence of the effective *g*-factor and linewidth derived from this fitting are shown in Fig. 3(b,c). The principal *g*-values of the anisotropic *g*-tensor shown in Fig. 3(b) remain almost temperature independent over the whole temperature range investigated with averaged values $g_{||}$ = 2.26±0.01 and $g_{\perp}$ = 2.12±0.01 resulting in g = 2.17±0.01, which is consistent with typical values for Cu^{2+} ions in other copper oxides.[20,21] The slight deviation of the *g*-factors from their high-temperature values below ~ 30 K, see Fig. 3(b), is indicative of the development of internal fields upon approaching the ordered phase.

The ESR linewidth $\Delta B_{||}$ demonstrates just small deviation from the almost constant value only below ~ 40 K (Fig. 2(c)), while the temperature dependence of linewidth for perpendicular component $\Delta B_{\perp}$ of anisotropic spectra is more obvious. The latter one increases with decreasing temperature and passes through a maximum at ~ 40 K. This behavior can be phenomenologically explained in terms of fluctuating internal field which adds to the applied field altering the resonance condition. The slowing down of the fluctuation rate of this field may produce a progressive broadening of the resonance line as the temperature decreases. The occurrence of such fluctuating fields might be traced to the noticeable short-range correlations in the system which is present at temperatures essentially higher the ordering temperature. The difference in behavior of $\Delta B_{||}$ (T) and $\Delta B_{\perp}$ (T) indicates that the correlations in Cu(OH)F are evolving in an anisotropic manner. Typically, ESR spectra tend to broaden monotonically upon lowering temperature as spin correlations develop. Nevertheless, the linewidth $\Delta B_{\perp}$ passes through a maximum and then decreases smoothly upon approaching the Néel temperature. Similar behavior was observed in Cu^{2+} based antiferromagnets,[22,23] it may reflect the saturation of the spin correlation length and the depletion of the spin fluctuation density.[24]

4. Thermodynamics

The temperature dependences of magnetic susceptibility χ in various samples of Cu(OH)F are shown in Fig. 4. At elevated temperatures, the magnetic susceptibility of Cu(OH)F follows the modified Curie-Weiss law

$$\chi = \chi_0 + \frac{C}{T - \Theta} \quad (2)$$

which takes into account the presence of temperature-independent term χ_0. The fit of $\chi(T)$ dependence in the range T = 200 - 300 K gives $\chi_0 = 2.15\times10^{-5}$ emu/mol, C = 0.44 emu/molK and Θ = 15 K. The temperature-independent contribution is due to summation of individual Pascal's constants of constituent ions in the structure of Cu(OH)F $\chi_0^{dia} = \sim 3.2\times10^{-5}$ emu/mol,[25] plus paramagnetic van Vleck contribution of Cu^{2+} ions χ^{vV}. This contribution is about 5.5×10^{-5} emu/mol in cupric coordination compounds.[26]

The value of Curie constant C defines the effective magnetic moment in Cu(OH)F as μ_{eff} = 1.87 μ_B which should be put into correspondence with the effective magnetic moment of free electron 1.73 μ_B. This, in turn, defines the g – factor as g = 2.17 which is in good agreement with experimentally found values in ESR measurements at room temperature. The positive Weiss temperature Θ indicates predominance of ferromagnetic interactions in the magnetic subsystem of Cu(OH)F at elevated temperatures. At lowering temperature, the contribution of antiferromagnetic exchange interactions rapidly strengthens, as shown in the Inset to Fig. 4.

In various samples of Cu(OH)F the temperature dependence of magnetic susceptibility demonstrates peak in the range T_N = 9.5 ÷ 11.5 K which indicates formation of static magnetic order. The spread in Neel temperature we attribute to the presence of some non-reproducible disorder in the structure of Cu(OH)F. At $T < T_N$, the field dependences of static magnetization, shown in Fig. 5, evidence anomalies typical for the spin-flop transition in polycrystalline sample. The pulsed field measurements of magnetization up to B = 31 T resulted in M_{sat} = 0.86 μ_B/f.u. at 2.4 K, indicating significant reduction of saturated magnetic moment in the ground state of Cu(OH)F. While the spin-flop transition at 2 K can be identified at ~ 3.5 T, no sharp spin-flip transition is seen in M vs. B dependence, as shown in the Inset to Fig. 5.

The transition into magnetically ordered state is further confirmed by specific heat measurements $C_p(T)$, as shown in Fig. 6. In contrast to standard lambda-type peak the phase transition in Cu(OH)F is seen as relatively broad anomaly at low temperatures. With increasing magnetic field the transition shifts to lower temperatures indicating rapid suppression of antiferromagnetic order. Fitting the phonon contribution by polynomials and extracting it from $C_p(T)$ curve allows estimating the magnetic entropy. The temperature dependence of magnetic entropy S is shown in the lower Inset to Fig. 6. It saturates only at the temperatures four times exceeding the ordering temperature. The magnetic entropy released in the whole temperature range 4.44 J/molK constitute about 80% of the expectancy value Rln2 = 5.76 J/molK. This roughly corresponds to reduction of Cu^{2+} magnetic moment seen in magnetization data. The magnetic phase diagram of Cu(OH)F extracted from $M(B)$ and $C_p(T)$ dependences is shown in the upper Inset to Fig. 6.

5. Muon-spin spectroscopy

The temperature evolution of the muon spin polarization P(t) in Fig. 7 shows a defined increase of the relaxation rate around 10 K indicative of the onset of static magnetism. Furthermore, the appearance of a minimum in the depolarization curves at lowest temperatures together with the increase to a 1/3 tail at longer times unambiguously proves the existence of static local fields. In a magnetically ordered polycrystalline sample 1/3rd of the muon spin component points along B_{loc} due to the powder average and does not undergo precession while the remaining 2/3rd component of the spin precesses around B_{loc}. Magnetic disorder results in a distribution of local magnetic fields B_{loc} and the precessing part of the polarization is damped with the transverse relaxation rate λ_T. If the magnetic disorder is strong λ_T becomes large and the oscillations over-damped. The phase transition is however still visible from the sharp increase of λ_T.[27] Because of the absence of a clear oscillation signal in Cu(OH)F the order can be described as rather short-ranged. The fact that a local minimum is visible in P(t) before the oscillations become over-damped allows to estimate a magnetic correlation length that is larger than about ten nearest neighbor Cu-Cu distances.[28]

To validate these observations the muon spin polarization measured in the temperature range 1.6 – 21.2 K was fitted to the following polarization function

$$P(t) = \frac{1}{3}e^{-\lambda_L t} + \frac{2}{3}e^{-(\lambda_T t)^{\beta}} \cos(\gamma_\mu B_{loc} t). \quad (3)$$

Here, B_{loc} is internal field at the muon site, γ_μ is the gyromagnetic ratio of the muon, λ_T and λ_L are the transverse and longitudinal relaxation rates respectively and β is the stretching exponent of the former. The fitted muon spin polarizations are shown by the black lines in Fig. 7. The transverse relaxation rate λ_T as a function of temperature is plotted in the inset of Fig. 7 together with the development of the internal magnetic field B_{loc}. The onset of static magnetism is clearly visible from the increase of λ_T and the development of a static internal field at the muon site below 10 K. The stretching exponent of the transverse relaxation rate approaches β=0.5 at the transition temperature showing a root exponential relaxation while it is almost Gaussian (β≈2) below and above the transition temperature. The relaxation below 10 K is explained by the static local fields while the relaxation above the transition is ascribed to a strong dipolar coupling between the muon spin and the fluorine nuclear spin. Positive muons implanted into materials containing F^- ions forms an F-μ-F bond with a characteristic relaxation function.[29] Additional dynamic fluctuations observed by the muon spin are described by a damping of non-precessing part of the polarization with the longitudinal relaxation rate λ_L. As expected, critical fluctuations near the phase transition are evident from an increase of λ_L at about 10 K in Cu(OH)F.

6. First Principles Calculations

In order to gain microscopic understanding, we carried out first principles density functional theory (DFT) calculations of Cu(OH)F. Calculations have been carried out using plane wave basis as implemented within Vienna Abinitio Simulation Package (VASP)[30] as well as muffin-tin orbital (MTO) based N-th order MTO (NMTO)[31] and linear MTO (LMTO)[32] calculations implemented in Stuttgart code.

The non-spin polarized density of states calculated within generalized gradient approximation (GGA) of exchange-correlation functional shows half-filled Cu d_{x2-y2} states crossing the Fermi level which is strongly admixed with O-*p* and F-*p* states, as shown in Fig. 7. Inclusion of missing correlation effect beyond GGA (+U) and spin-polarization makes the system insulating in agreement with experimental observation.

Using NMTO-downfolding procedure, we construct the effective Cu d_{x2-y2} Wannier function by keeping active only Cu d_{x2-y2} degrees of freedom, and integrating out all other degrees of freedom. Fig. 8 shows the plot of this Wannier function which has the central part shaped according to d_{x2-y2} symmetry and the tails shaped according to integrated out O-*p* and F-*p* degrees of freedom. Finite mixing with H-*s* character makes the lobes of the O-*p* like tails asymmetric. We further see that the wavefunction extends to neighboring layers, in terms of weights at O and F in the neighboring planes suggesting rather three dimensional nature of the compound. Construction of the real-space Hamiltonian in the effective Cu d_{x2-y2} Wannier function basis provides the information of effective Cu-Cu hopping interactions which appears to be rather long ranged. The predominant interactions are, t_1, the inplane Cu-Cu interaction via two O, t_2, the inplane Cu-Cu coupling via one F and one O, t_3, the inplane Cu-Cu interaction via two F, and two out of plane interactions, t_5 and t_6, which proceeds through interaction between H in a given plane and F or O in the neighboring plane. t_4, the inplane Cu-Cu coupling via one F and one O forming a part of the uniform chain, is found to be small. The corresponding magnetic interactions, J1 – J6, are shown in Fig. 9. We carried out total energy calculations of a 2×1×2 supercell containing a total of 16 Cu atoms for 12 different spin configurations in GGA+U scheme with choice of U = 8 eV. Different J values were extracted by mapping the total energies of the different magnetic configurations into a Heisenberg model. The precise values of J's turn out to rather sensitive to choice of magnetic configurations suggesting highly competitive nature of different magnetic interactions. The general trend is found as follows, J1 is of antiferromagnetic (AFM) nature, J2 is AFM while J3 is ferromagnetic (FM). The out of plane interaction J6 is FM while J5 is AFM. This clearly shows the presence of competing FM and AFM interactions. Calculating J_{eff} defined as $\Sigma J_i z_i$ (z_i being the number of neighbors for a given interaction) we find a small AFM value

of $J_{eff,}$ (~ 2-5 meV) the precise value being dependent on the precise choice of set of J's. This stresses once again the delicate balance between competing interactions present in this compound. This should give an ordering temperature of the order of tens of Kelvin, as found experimentally.

7. Conclusion

Basing on available data it is difficult to judge which magnetic configuration is realized in Cu(OH)F. Rather broad anomaly in $C_p(T)$ dependence at phase transition and smeared magnetization saturation curve M(B) at low temperatures suggest some disorder in the ground state. The presented zero-field μSR data are consistent with Cu(OH)F experiencing a transition into a static but magnetically short range state. The critical temperature obtained in μSR measurements is slightly lower than the center of the broad maxima observed in the specific heat and dc-susceptibility data at around 11.5 K.

Surprisingly, the properties of isostructural compounds, Cu(OH)Cl and Cu(OH)F, appear to be quite different. In cupric hydroxide chloride the anomalies in magnetic susceptibility and specific heat are quite sharp as compared to those in cupric hydroxide fluoride. Unlike situation in Cu(OH)F, the specific heat anomaly in Cu(OH)Cl is virtually non-sensitive to magnetic field and the magnetization is very far from saturation even at 60 T.[18)] Tentatively, this can be attributed at least partially to the difference of O/F and O/Cl ionic size ratio which allows or prevents the mutual substitutions.

One more mixed anion cupric compound to be compared with is $Cu_2(OH)_3Cl$ which exists in three distinct polymorphs, atacamite,[33)] botallackite[34)] and clinoatacamite.[35)] Atacamite undergoes an antiferromagnetic transition at T_N = 9 K having disordered magnetic ground state. In contrast, botallackite possesses long-range magnetic order below T_N = 7.2 K. The clinoatacamite undergoes an antiferromagnetic transition at T_N = 18.1 K, below 6.4 K it transits into a disordered spin-glass-like state. The variations in copper coordination and geometric frustration of the quantum Cu^{2+} spins are suggested to be responsible for the formation of these disordered and ordered phases.[36,37)]

Overall, the magnetism of mixed anion transition metal compounds represents largely uninvestigated field. The chemical disorder with regards to positions of halide and hydroxide ions may provoke magnetic disorder at low temperatures. The powerful microscopic probes including nuclear magnetic resonance and neutron scattering seems to be necessary to establish quantum ground states in these seemingly simple compounds.

Acknowledgement

This work was supported in part from the Ministry of Education and Science of the Russian Federation in the framework of Increase Competitiveness Program of NUST «MISiS» (№ К2-2014-036). AP and EZ acknowledge support from Russian Foundation for Basic Research Grant № 14-02-00245.

* Email: t.sahadasgupta@gmail.com (theory)
# Email: vasil@mig.phys.msu.ru(experiment)

References:

1. B. Raveau, C. Michel, M. Hervieu, and D. Groult, Crystal Chemistry of High-Tc Superconducting Copper Oxides. Springer Verlag, 1991.
2. A.F. Wells, Structural Inorganic Chemistry. Clarendon Press, Oxford, 1984.
3. W. Geertsma and D. Khomskii, Phys. Rev. B 54, 3011 (1996).
4. T. Kimura, Y. Sekio, H. Nakamura, T. Siegrist and A.P. Ramirez, Nature Materials **7**, 291 (2008).
5. S. Seki, T. Kurumaji, S. Ishiwata, H. Matsui, H. Murakawa, Y. Tokunaga, Y. Kaneko, T. Hasegawa, and Y. Tokura, Phys. Rev. B **82**, 064424 (2010).
6. C. Lee, J. Liu, M.-H. Whangbo, H.-J. Koo, R.K. Kremer, and A. Simon, Phys. Rev. B 86, 060407 (2012).
7. Non-Tetrahedrally Bonded Elements and Binary Compounds I. Landolt-Börnstein – Group III Condensed Matter, Vol. 41C, Springer Verlag, 1998.

8. R. Villarreal, G. Quirion, M.L. Plumer, M. Poirier, T. Usui, and T. Kimura, Phys. Rev. Lett. **109**, 167207 (2012).
9. A. Rebello, Z.C.M. Winter, S. Viall, and J.J. Neumeier, Phys. Rev. B **88**, 094420 (2012).
10. M.G. Banks, R.K. Kremer, C. Hoch, A. Simon, B. Ouladdiaf, J.-M. Broto, H. Rakoto, C. Lee, and M.-H. Whangbo,Phys. Rev. B **80**,024404 (2009).
11. L. Zhao, T.-L. Hung, C.-C. Li, Y.-Y. Chen, M.-K. Wu, R.K. Kremer, M.G. Banks, A. Simon, M.-H. Whangbo, C. Lee, J.S. Kim, I. Kim, and K.H. Kim, Adv. Mater. **24**, 2469 (2012).
12. R.J. Joenk and R.M. Bozorth, J. Appl. Phys. **36**, 1167 (1965).
13. P. Reinhardt, M.P. Habas, R. Dovesi, I. de P.R. Moreira, and F. Illas, Phys. Rev. B **59**, 1016 (1999).
14. H.R. Oswald, A. Reller, H.W. Schmalle, and E. Dubler, Acta Cryst. C **46**, 2279 (1990).
15. P. Umek, J.W. Seo, L. Fórró, P. Cevc, Z Jagličič, M. Škarabot, A. Zorko, and D. Arčon, AIP Conf. Proc. **723**, 427 (2004).
16. M. Diot, P. Turlier, and J.-C. Volta, C. R. Acad. Sci. B**, 274**, 225 (1972).
17. Y. Cudennec, A. Riou, Y. Gerault, and A. Lecerf, J. Sol. St. Chem. **151**, 308 (2000).
18. T. Pungas, Master's Thesis, Tartu 2014.
19. G. Giester, E. Libowitzky, Z. Kristallogr. **218**, 351 (2003).
20. A. Abragam, B. Bleaney, *Electron paramagnetic resonance of transition ions*, Clarendon Press, Oxford, 1970.
21. R.M. Krishna and S.K. Gupta, Bull. Magn.Resonance,16, 239 (1994).
22. K. V. Zakharov, E. A. Zvereva, P. S. Berdonosov, E. S. Kuznetsova, V. A. Dolgikh, L. Clark, C. Black, P. Lightfoot, W. Kockelmann, Z. V. Pchelkina, S. V. Streltsov, O. S. Volkova, and A. N. Vasiliev, Phys. Rev. B **90**, 214417 (2014).
23. L. Shvanskaya, O. Yakubovich, A.Ivanova, S.Baidya, T.Saha-Dasgupta, E.Zvereva, A. Golovanov, O.Volkova, and A.Vasiliev, New J. Chem. **37**, 2743 (2013).
24. F. Chabre, A.M. Ghorayeb, P. Millet, V.A. Pashchenko, and A. Stepanov, Phys. Rev. B **72**, 012415 (2005).
25. G.A. Bain and J.F. Berry, J. Chem. Educ., **85**, 532 (2008).
26. H. Lueken, Magnetochemie (Teubner, Leipzig, Germany, 1999).
27. Y.J. Uemura, T. Yamazaki, D.R. Harshman, M. Senba, and E.J. Ansaldo, Phys. Rev. B **31**, 546 (1985).
28. Alain Yaouanc and Pierre Dalmas de Rotier, *Muon Spin Rotation, Relaxation and Resonance* (Oxford University Press, 2011).
29. J.H. Brewer, S.R. Kreitzman, D.R. Noakes, E.J. Ansaldo, D.R. Harshman, and R. Keitel, Phys. Rev. B **33**, 7813 (1986).
30. G. Kresse et. al., Phys. Rev. B **54**, 11169 (1996).
31. O. K. Andersen and T. Saha-Dasgupta, Phys. Rev. B **62**, R16219 (2000).
32. O. K. Andersen and O. Jepsen, Phys. Rev. Lett. **53**, 2571 (1984).
33. J.B. Parise and B.G. Hyde, Acta Cryst. C, **42**, 1277 (1986).
34. F. C. Hawthorne, Miner. Mag. **49**, 87 (1985).
35. J.D. Grice, J.T. Szymanski and J.L. Jambor, Can. Mineral. **34**, 73 (1996).
36. X.G. Zheng, T. Mori, K. Nishiyama, W. Higemoto, H. Yamada, K. Nishikubo, and C. N. Xu, Phys. Rev. B **71**, 174404 (2005).
37. X.G. Zheng, T. Kawae, Y. Kashitani, C.S. Li, N. Tateiwa, K. Takeda, H. Yamada, C.N. Hu, and Y. Ren, Phys. Rev. B **71**, 052409 (2005).

Figure captions

Fig. 1. The crystal structure of Cu(OH)F in polyhedral representation in *bc* plane. The hydrogen ions are shown by green unbounded circles.

Fig. 2. Evolution of the ESR spectra with temperature in Cu(OH)F: the circles are experimental data, the lines are fits of the data as described in the text.

Fig. 3. (a) The representative example of ESR spectra (circles) decomposition at 40 K with the fits to the data as described in the text shown by the lines. The dashed and dash-dotted lines show the individual Lorentzian fit components and the solid line is the sum of two components. (b) The temperature dependence of principal values of *g*-tensor. (c) The temperature dependence of the ESR linewidth for two resolved components of the ESR spectra in Cu(OH)F.

Fig. 4. The temperature dependences of magnetic susceptibility in various samples of Cu(OH)F at B = 0.1 T. The fit by Curie-Weiss law is shown by solid line. Inset: the temperature dependences of Curie constant $C = (\chi-\chi 0)/(T-\Theta)$. The dashed line represents the limiting value C = 0.44 emu/molK.

Fig. 5. The field dependences of magnetization in Cu(OH)F in the range T = 2 – 20 K. Inset: the pulsed field magnetization curve at T = 2.4 K.

Fig. 6. The temperature dependences of specific heat in Cu(OH)F taken at various magnetic fields in the range B = 0 – 9 T. The dashed line represents the phonon contribution. Lower Inset: the temperature dependence of magnetic entropy S. Upper Inset: the magnetic phase diagram of Cu(OH)F.

Fig**. 7.** Time-dependent muon spin polarization P(t) of Cu(OH)F at selected temperatures measured in zero-field. Solid lines are fits to the data using equation (3). The inset shows the temperature dependence of the fit parameters internal field Bloc and transverse relaxation rate λ_T.

Fig. 8. Non-spin polarized GGA density of states of Cu(OH)F projected onto Cu d, O p, F *p* and H *s* states. Zero of the energy is set at Fermi energy.

Fig. 9. The plot of effective Cu d_{x2-y2} Wannier function. The oppositely signed lobes of the wavefunction are colored as orange and violet. Plotted is the isovalue surface. The black, red, cyan, small green balls represent positions of Cu, O, F and H in the structure.

Fig. 10. Various intra- and inter-layer Cu-Cu magnetic exchanges in Cu(OH)F. The black, red, cyan and green balls represent Cu, O, F and H atoms.

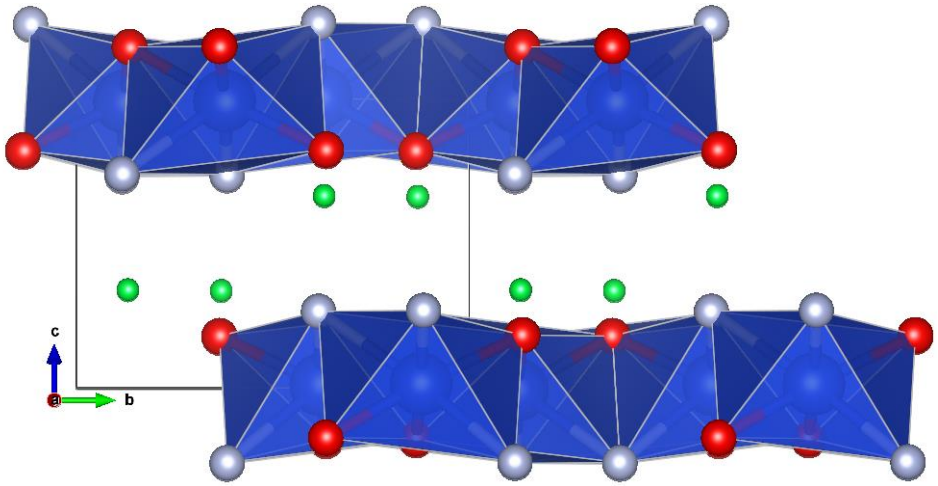
c
b

Fig. 1.

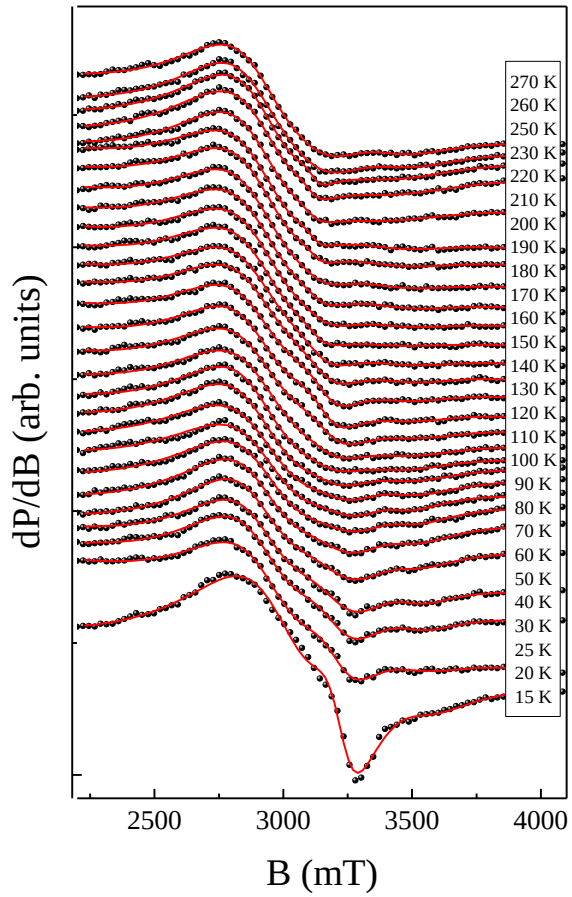
dP/dB (arb. units)
B (mT)
2500
3000
3500
4000
270 K
260 K
250 K
230 K
220 K
210 K
200 K
190 K
180 K
170 K
160 K
150 K
140 K
130 K
120 K
110 K
100 K
90 K
80 K
70 K
60 K
50 K
40 K
30 K
25 K
20 K
15 K

Fig. 2.

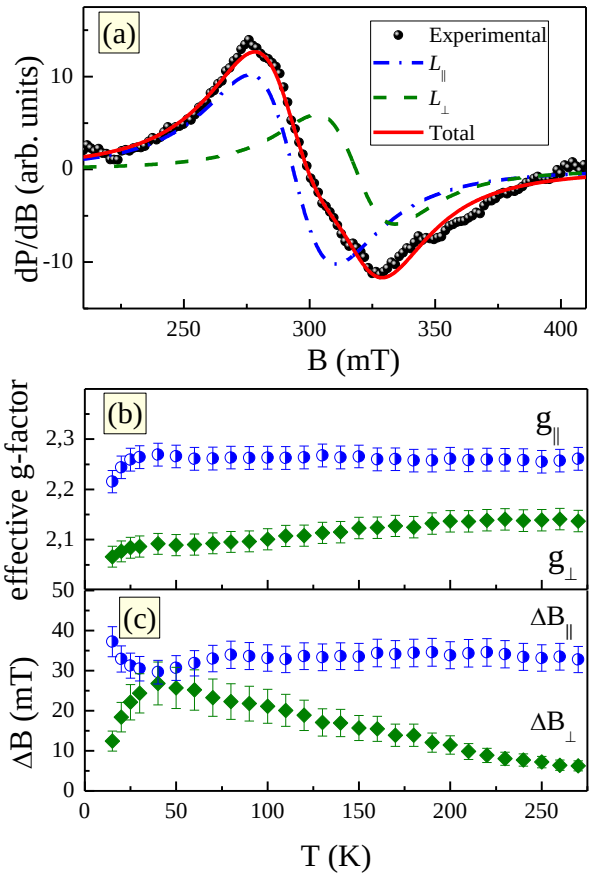
(a)
Experimental
$L_{\parallel}$
$L_{\perp}$
Total
dP/dB (arb. units)
B (mT)
(b)
$g_{\parallel}$
$g_{\perp}$
effective g-factor
(c)
$\Delta B_{\parallel}$
$\Delta B_{\perp}$
ΔB (mT)
T (K)

Fig. 3.

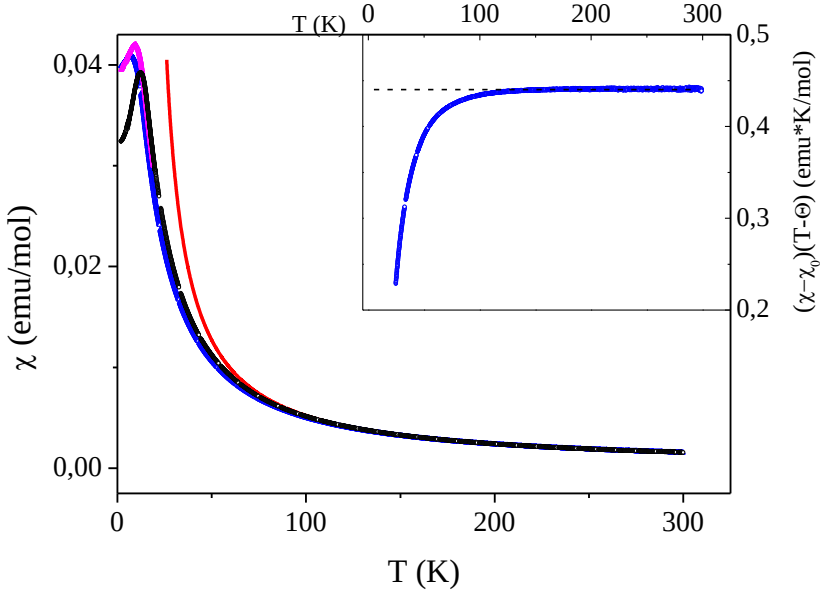
T (K)
χ (emu/mol)
$(\chi-\chi_0)(T-\Theta)$ (emu*K/mol)
T (K)

Fig. 4.

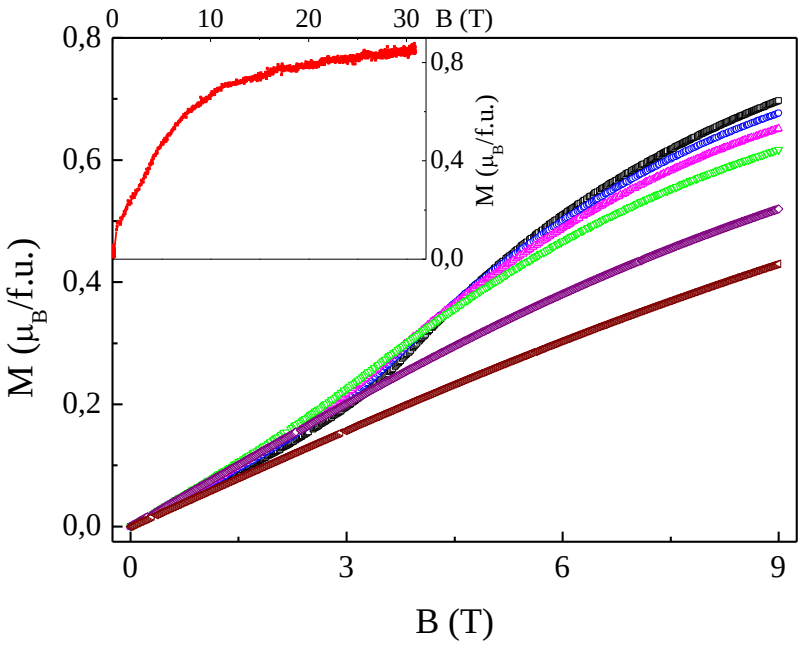
0 10 20 30 B (T)
0,8
0,6
0,4
0,2
0,0
M (μ_B/f.u.)
0,8
0,4
0,0
M (μ_B/f.u.)
0 3 6 9
B (T)

Fig. 5.

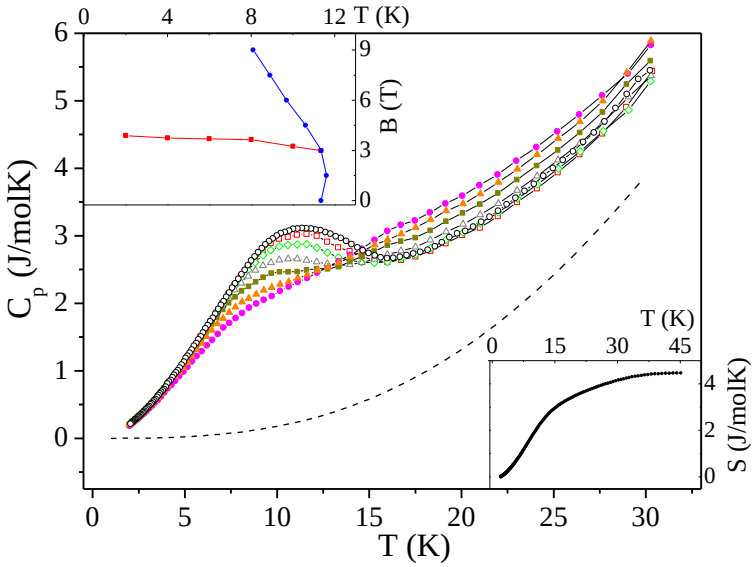
0 4 8 12 T (K)
9
6
3
0
B (T)
6
5
4
3
2
1
0
C_p (J/molK)
T (K)
0 15 30 45
4
2
0
S (J/molK)
0 5 10 15 20 25 30
T (K)

Fig. 6.

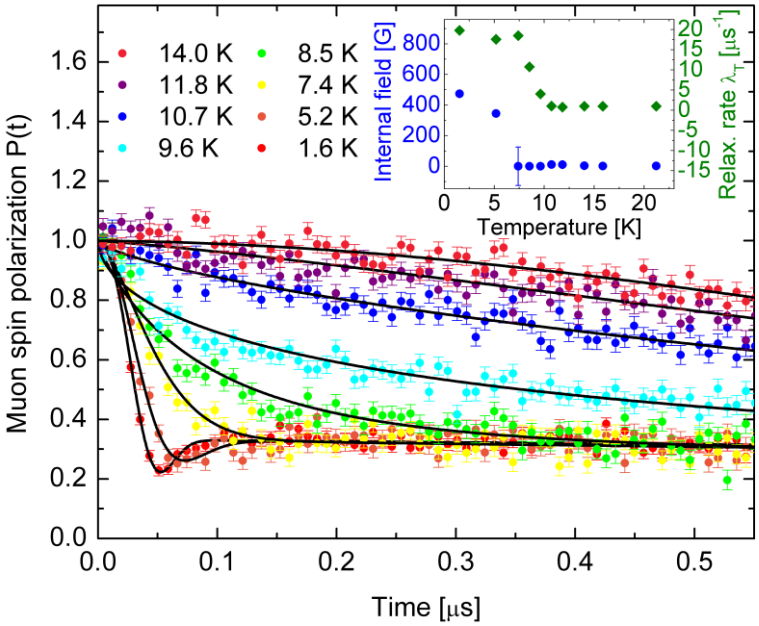

Fig. 7.

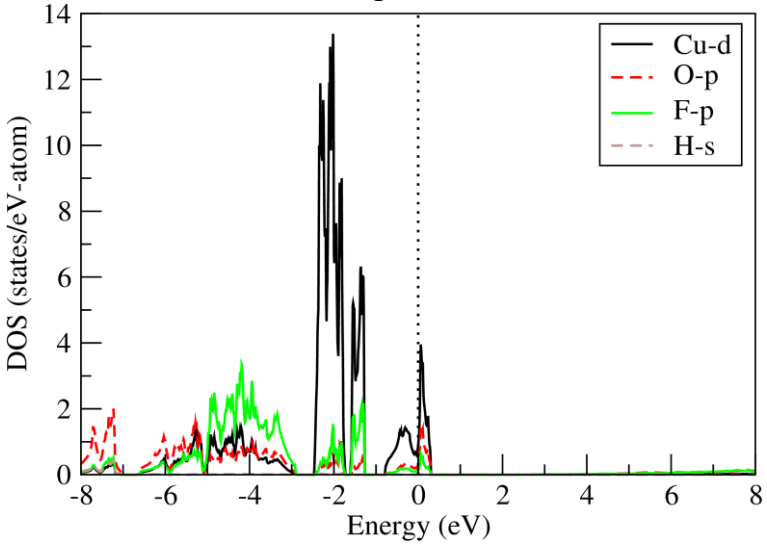

Fig. 8.

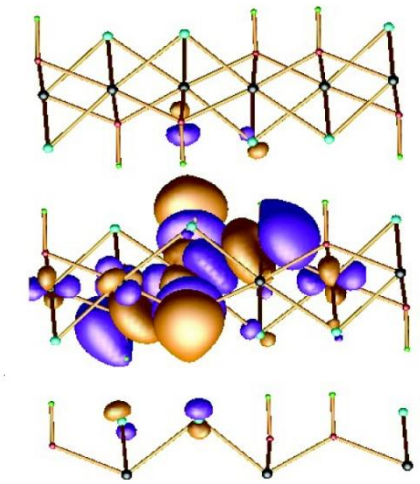

Fig. 9.

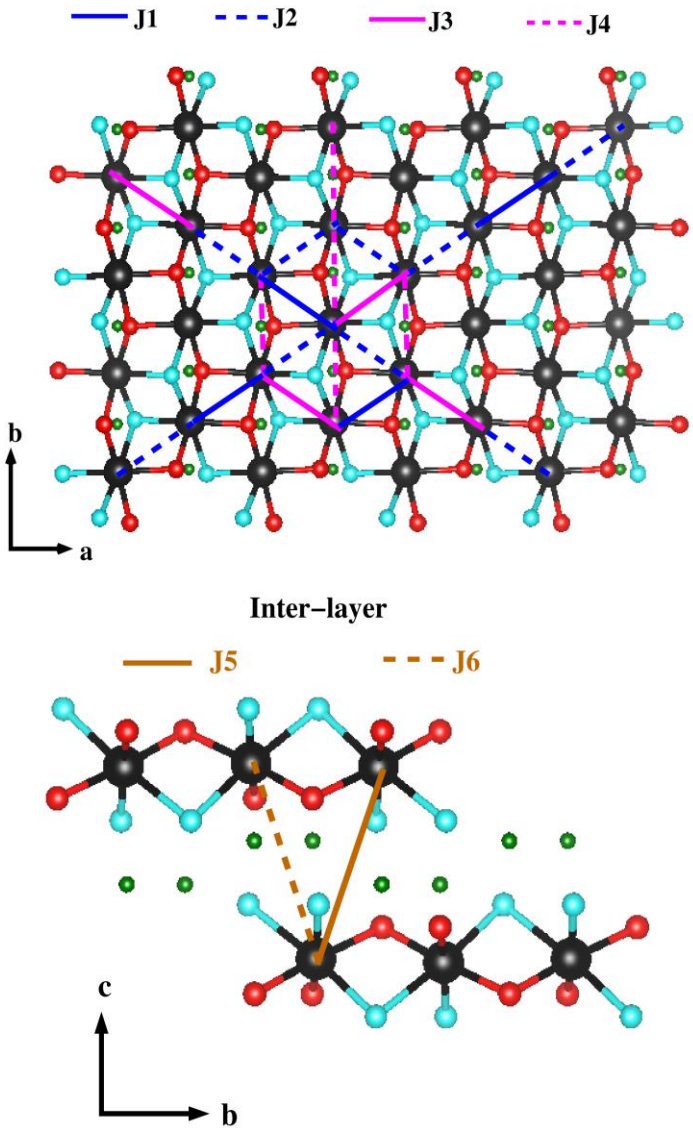

Fig. 10.